JGR Space Physics

RESEARCH ARTICLE
10.1029/2024JA032626

O-Mode Instability for Non-Thermal Continuum Radiation Generated Near the Plasmapause

Chio Z. Cheng[1], Eun-Hwa Kim[1,2], Scott A. Boardsen[3,4], Iver H. Cairns[5], and Jay R. Johnson[6]

[1]Princeton Plasma Physics Laboratory, Princeton University, Princeton, NJ, USA, [2]Department of Physics, Andrews University, Berrien Springs, MI, USA, [3]NASA Goddard Space Flight Center, Greenbelt, MD, USA, [4]Goddard Planetary Heliophysics Institute, University of Maryland in Baltimore, Baltimore, MD, USA, [5]School of Physics, University of Sydney, Sydney, NSW, Australia, [6]School of Engineering, Andrews University, Berrien Springs, MI, USA

Key Points:

- The ordinary mode electron anisotropy instability is examined to comprehend the non-thermal continuum radiation near the plasmapause
- Resonant ordinary modes are unstable over multiple narrow frequency and wavevector ranges
- NTC radiation generated by the instability near the plasmapause can propagate nearer to the magnetic equator

Correspondence to:
E.-H. Kim,
ehkim@pppl.gov

Citation:
Cheng, C. Z., Kim, E.-H., Boardsen, S. A., Cairns, I. H., & Johnson, J. R. (2024). O-mode instability for non-thermal continuum radiation generated near the plasmapause. *Journal of Geophysical Research: Space Physics*, *129*, e2024JA032626. https://doi.org/10.1029/2024JA032626

Received 10 MAR 2024
Accepted 17 SEP 2024

Author Contributions:
Conceptualization: Eun-Hwa Kim, Scott A. Boardsen
Formal analysis: Chio Z. Cheng
Funding acquisition: Eun-Hwa Kim
Investigation: Chio Z. Cheng, Eun-Hwa Kim
Methodology: Chio Z. Cheng
Project administration: Eun-Hwa Kim
Supervision: Eun-Hwa Kim
Visualization: Eun-Hwa Kim
Writing – original draft: Chio Z. Cheng, Eun-Hwa Kim
Writing – review & editing: Eun-Hwa Kim, Scott A. Boardsen, Iver H. Cairns, Jay R. Johnson

Abstract Analysis of the ordinary mode (O-mode) instability is performed to comprehend the nonthermal continuum (NTC) radiation near the plasmapause, taking into account the relativistic wave-electron resonance effect. The energy source is the anisotropy in the velocity of the minority suprathermal electron population. Numerical solutions demonstrate that the O-mode can be unstable with multiple narrow frequency bands located close to harmonics of the electron cyclotron frequency above the local electron plasma frequency. These waves have narrow beaming angle bands of nearly 90° relative to the ambient magnetic field. Our findings indicate that NTC radiation generated by this wave-electron resonance instability near the plasmapause can propagate nearer to the magnetic equator with multiple harmonics, which is in agreement with a recent statistical study using Van Allen Probes.

1. Introduction

Non-thermal continuum (NTC) radiation, which is associated with strong density gradients, non-thermal electrons, and upper hybrid waves, has often been detected at Earth and magnetized planets (Boardsen et al., 2008, 2023; Décréau et al., 2004, 2015; Green & Boardsen, 1999; Grimald et al., 2007; Gurnett, 1975; Gurnett et al., 1988; Hashimoto et al., 1999, 2005; Kasaba et al., 1998; Kurth & Gurnett, 1991; Kurth et al., 2016; Louis et al., 2021; Morgan & Gurnett, 1991; S. Y. Wu et al., 2022; Ye et al., 2009, 2010). At Earth, NTC radiation is generated over a broadband frequency range from a few hundred to several hundred kHz. Because NTC radiation can freely escape from the Earth's magnetosphere at frequencies above the magnetopause electron plasma frequency, this emission has been referred to as escaping continuum radiation (Kurth et al., 1981). Continuum radiation in the 100–800 kHz frequency range is identified as kilometric continuum (KC) radiation (Hashimoto et al., 1999).

Escaping NTC radiation is generated near the plasmapause, a region with a strong density gradient (Gurnett, 1975; Kurth et al., 1981) and KC radiation is also observed to be associated with density depletions or notch structures in the plasmasphere as well as near the plasmapause (Green et al., 2002, 2004; Hashimoto et al., 1999). The NTC and KC emission is radiated obliquely with the beaming angle (Θ) $40° \leq \Theta < 90°$(Morgan & Gurnett, 1991). However, these radiations are occasionally detected near the magnetic equator with $\Theta \approx 90°$ (Boardsen et al., 2008, 2023; Hashimoto et al., 2005). The radiation patterns of both KC and escaping NTC radiation have large longitudinal extents and often exhibit harmonics in their frequency spectra (Décréau et al., 2015; Grimald & Santolík, 2010; Morgan & Gurnett, 1991).

For many years, the origin of this radiation has been studied, yet its primary source remains unknown. It could be produced either directly by local plasma instabilities or indirectly through a process such as linear or nonlinear mode conversion. Linear mode conversion (LMC) theory is widely accepted as the generation mechanism for NTC and KC radiation. In this theory, when the plasma density gradient is nearly perpendicular to the magnetic field ($\mathbf{B}_0$), upper-hybrid (UH) electrostatic (ES) waves convert to Z-mode radiation which converts to ordinary-mode (O-mode) free space electromagnetic (EM) waves at a frequency close to the electron plasma frequency ($\omega \approx \omega_{pe}$) (Budden & Jones, 1987; Jones, 1980; Kalaee & Katoh, 2020; Kim et al., 2007, 2008, 2013; Oya, 1971; Schleyer et al., 2013, 2014). This process results in two symmetric free space beams in magnetic latitude propagating in the lower-density region in both the northern and southern hemispheres (Gurnett et al., 1988; Jones, 1980; Jones et al., 1987). Although not pertinent to this study, we note that the LMC theory beaming angle

can be modified when the angle between the density gradient and $\mathbf{B}_0$ is not perpendicular (Budden, 1980; Kalaee & Katoh, 2016a, 2016b; Kalaee et al., 2014).

A recent statistical analysis of the NTC beaming angles using the Van Allen Probes computed over the entire mission (Boardsen et al., 2023) has provided strong evidence in favor of LMC theory in the lower frequency range (17−100 kHz). In this frequency range, mission-duration scatter plots of beaming angle versus magnetic latitude form an inverted V pattern with the apex at the magnetic equator. Such a pattern is predicted by LMC theory for large statistical studies covering multiple years and orbits due to the variation of the plasmapause location. However, for higher frequencies (100−400 kHz) this pattern was weakly observed, with the bulk of the beaming angles strongly concentrated near 90° to the magnetic field. KC studies by Hashimoto et al. (2005) and Boardsen et al. (2008) also concluded that the beaming angle was directed much closer to the equatorial plane than that predicted by LMCT.

Nonlinear theories have proposed a three-wave interaction to generate energy in the free space wave mode (Fung & Papadopoulos, 1987; Melrose, 1981; Rönnmark, 1983). Fung and Papadopoulos (1987) showed that two UH-branch ES waves can create daughter EM waves, which can propagate quasi-perpendicular to $\mathbf{B}_0$, which is similar to the KC radiation detected near the magnetic equator (Boardsen et al., 2008, 2023; Hashimoto et al., 2005).

The direct generation of O-mode due to suprathermal electrons can also potentially explain the multiple harmonics of the NTC (Cheng, 1975; Farrell, 2001; Freund & Wu, 1976; Gaffey et al., 1972, 1973; Shi et al., 1986; C. S. Wu & Lee, 1979). Cheng (1975) investigated the O-mode instability with a finite real frequency (ω_r) near the electron cyclotron harmonics for waves propagating perpendicular to $\mathbf{B}_0$. He demonstrated that the non-resonant O-mode could be unstable under conditions of high $\beta_{\|}$ and growth rates (γ) comparable to the cyclotron frequency (ω_{ce}) when suprathermal electrons with ring distributions in the perpendicular velocity and a counter streaming Maxwellian distribution in the parallel velocity were adopted.

The effects of relativity on the wave-particle resonance were also studied (Freund & Wu, 1976; C. S. Wu & Lee, 1979). Freund and Wu (1976) found that the O-mode can become weakly unstable $(\gamma \ll \omega_{ce})$ at low $\beta_{\|}$ and $T_{\|} < T_{\perp}$, where $T_{\|(\perp)}$ is the electron temperature parallel (perpendicular) to $\mathbf{B}_0$. C. S. Wu and Lee (1979) used a perturbative approach $(\gamma \ll \omega_r)$ for a suprathermal electron loss cone distribution to show that the quasi-perpendicular propagating O-mode can be unstable due to the relativistic wave-particle resonance. Later, Farrell (2001) proposed that O-mode emission can be generated by mildly energetic electron beams (1 − 10 keV) in a highly dense $(\omega \sim \omega_{pe} \gg \omega_{ce})$ warm plasma. He demonstrated that the resonant O-mode instability mechanism can generate narrow-banded EM electron cyclotron harmonic emissions at the magnetopause. Recent numerical simulations also demonstrated that electrostatic emission caused by ring instability can generate O-mode waves that can be emitted at an oblique angle (Horký & Omura, 2019; Horký et al., 2018).

Previous research on the direct generation mechanism demonstrated O-mode generation and applied theories for terrestrial continuum radiations, but no examination of NTC generation near the plasmapause has been conducted. This paper investigates the generation of NTC and KC near the plasmapause by providing numerical solutions of the O-mode instability with finite wavenumber parallel to $\mathbf{B}_0$ when the relativistic wave-particle resonance with suprathermal electrons at the plasmapause is considered. Spacecraft observations have revealed that the electron velocity distribution consists of a core thermal component and a suprathermal component during intense upper hybrid wave activities near the magnetic equator. The detected suprathermal electron distribution shows weak ring distributions with a positive slope in velocity perpendicular to $\mathbf{B}_0$ (Figure 2 of Sentman et al. (1979) and Figure 3 of Kurth et al. (1979)) and the same with the addition of counterstreaming parallel beam features with positive slope (Figure 2 of Kurth et al. (1980)). Thus, we consider mildly energized electrons with perpendicular ring and parallel counter streaming Maxwellian velocity distributions (Cheng, 1975). Numerical surveys of the O-mode instability are also presented, showing how each physical parameter affects the O-mode generation.

This paper is organized as follows. Section 2 presents the relativistic O-mode wave dispersion relation, which is solved using ring- and counter streaming velocity distributions. The cutoff conditions of unstable O-mode generation for each cyclotron harmonic number are then calculated. Section 3 numerically solves the real wave frequency and the growth rate and examines the effect of each physical parameter on the wave growth rate. The last section discusses the wave generation at the plasmapause using typical plasmapause parameters and includes a summary.

2. Relativistic O-Mode Wave Dispersion With Suprathermal Electrons

By including the relativistic effect only in the resonance denominator, the O-mode dispersion equation is given by (Freund & Wu, 1976; C. S. Wu & Lee, 1979)

$$\begin{aligned}\omega^2 - k_\perp^2 c^2 = {} & 2\pi\sum_s \omega_{ps}^2 \int_{-\infty}^{\infty} dv_\parallel \int_0^{\infty} dv_\perp \left[v_\parallel^2 \frac{\partial f_{s0}}{\partial v_\perp} - v_\perp v_\parallel \frac{\partial f_{s0}}{\partial v_\parallel} \right] \\ & + 2\pi\sum_s \omega_{ps}^2 \int_{-\infty}^{\infty} dv_\parallel \int_0^{\infty} dv_\perp \left[(\omega - k_\parallel v_\parallel) \frac{\partial f_{s0}}{\partial v_\perp} + k_\parallel v_\perp \frac{\partial f_{s0}}{\partial v_\parallel} \right] \\ & \times \sum_{n=-\infty}^{\infty} \frac{v_\parallel^2 J_n^2}{k_\parallel v_\parallel + n\omega_{cs}(1 - v^2/c^2)^{1/2} - \omega},\end{aligned} \tag{1}$$

where $\omega \equiv \omega_r + i\gamma$, ω_r is a real frequency, γ is a growth rate, $k_{\parallel(\perp)}$ and $v_{\parallel(\perp)}$ are the components of the wave vector and electron velocity parallel (perpendicular) to $\mathbf{B}_0$, $\mathbf{v}$ is the particle velocity, $f_{0s}(v_\parallel, v_\perp)$ is the particle distribution function of particle species s, ω_{ps} and ω_{cs} are the plasma and cyclotron frequencies for particle species s, n is a cyclotron harmonic number, and J_n is the order n Bessel function of the first kind with an argument of $k_\perp v_\perp/\omega_{cs}$, respectively. Here, the relativistic resonance condition for particle species s is derived as

$$\omega - k_\parallel v_\parallel = n\omega_{cs}\sqrt{1 - v^2/c^2}. \tag{2}$$

To include the effects of suprathermal electron effects on the O-mode dispersion equation, the plasma is assumed to consist of core cold electrons and minor suprathermal electrons. Then, the electron density (n_e) is the sum of the core cold electron densities (n_c) and suprathermal (n_h) electron densities, $n_e = n_c + n_h$. The suprathermal electron velocity distribution function (f_{eh}) is chosen to be $f_{eh} = f_{e\parallel} f_{e\perp}$, where $f_{e\parallel(\perp)}$ is the parallel (perpendicular) velocity distribution. We assume that the parallel velocity distribution $f_{e\parallel}$ is a counter streaming Maxwellian distribution with parallel drift velocities $\pm u$ and the perpendicular velocity distribution $f_{e\perp}$ is a delta function ring distribution, respectively:

$$f_{e\parallel}(v_\parallel) = \left(2\sqrt{\pi}\, v_{e\parallel}\right)^{-1} \left[\exp\left(-\frac{(v_\parallel - u)^2}{v_{e\parallel}^2} \right) + \exp\left(-\frac{(v_\parallel + u)^2}{v_{e\parallel}^2} \right) \right], \tag{3}$$

$$f_{e\perp}(v_\perp) = (2\pi v_{\perp 0})^{-1} \delta(v_\perp - v_{\perp 0}), \tag{4}$$

where $v_{e\parallel}$ is the parallel thermal speed of the suprathermal electrons and $v_{\perp 0}$ is the perpendicular ring speed of the suprathermal electrons, respectively. Here, $f_{e\perp}$ is similar to the previous calculations (Cheng, 1975; Freund & Wu, 1976).

Then, the O-mode dispersion equation becomes,

$$\begin{aligned}\omega^2 = {} & \omega_{pe}^2 + k_\perp^2 c^2 \\ & - \omega_{ph}^2 \left(1 + \zeta_0^2 \left[2 + (\zeta_0 - t_e) Z(\zeta_0 - t_e) + (\zeta_0 + t_e) Z(\zeta_0 + t_e)\right]\right) J_0^2 \\ & + \omega_{ph}^2 \frac{v_{e\parallel}^2/2 + u^2}{v_{\perp 0}} \frac{\partial J_0^2}{\partial v_{\perp 0}} \\ & - \omega_{ph}^2 \sum_{n=1}^{\infty} \frac{2k_\parallel^2 c^2}{k_\parallel^2 c^2 + n^2 \omega_{ce}^2} \left[\frac{A_n J_n^2}{\zeta_{n+} - \zeta_{n-}} - \frac{v_{e\parallel}^2}{v_{\perp 0}} \frac{\partial}{\partial v_{\perp 0}} \left(\frac{B_n J_n^2}{\zeta_{n+} - \zeta_{n-}} \right) \right],\end{aligned} \tag{5}$$

where $\omega_{pe(ph)}$ is the electron (suprathermal) plasma frequency, Z is the plasma dispersion function, and the argument of the J-Bessel functions is $k_\perp v_{\perp 0}/\omega_{ce}$. The coefficients A_n and B_n in the summation over n are given by

$$
\begin{aligned}
A_n = & \left(\zeta_{n+} - \zeta_{n-}\right) \\
& + \left(\zeta_{n+} - \zeta_0\right)\zeta_{n+}^2\left[2 + \left(\zeta_{n+} - t_e\right)Z\left(\zeta_{n+} - t_e\right) + \left(\zeta_{n+} + t_e\right)Z\left(\zeta_{n+} + t_e\right)\right] \\
& - \left(\zeta_{n-} - \zeta_0\right)\zeta_{n-}^2\left[2 + \left(\zeta_{n-} - t_e\right)Z\left(\zeta_{n-} - t_e\right) + \left(\zeta_{n-} + t_e\right)Z\left(\zeta_{n-} + t_e\right)\right],
\end{aligned} \tag{6}
$$

$$
\begin{aligned}
2B_n = & \left(\zeta_{n+} - \zeta_{n-}\right)\left(1 + 2t_e^2\right) \\
& + \left(\zeta_{n+} - \zeta_0\right)^2\zeta_{n+}\left[2 + \zeta_{n+}Z\left(\zeta_{n+} - t_e\right) + \zeta_{n+}Z\left(\zeta_{n+} + t_e\right)\right] \\
& - \left(\zeta_{n-} - \zeta_0\right)^2\zeta_{n-}\left[2 + \zeta_{n-}Z\left(\zeta_{n-} - t_e\right) + \zeta_{n-}Z\left(\zeta_{n-} + t_e\right)\right],
\end{aligned} \tag{7}
$$

where $\zeta_0 \equiv \omega/k_\parallel v_{e\parallel}$, $t_e \equiv u/v_{e\parallel}$, and $\zeta_{n\pm} \equiv v_{n\pm}/v_{e\parallel}$, respectively. Here, $v_{n\pm}$ is the suprathermal electron resonant parallel velocity for each integer n and can be determined when the suprathermal electron resonance condition is satisfied,

$$
\left(\omega - k_\parallel v_{n\pm}\right)^2 + n^2\omega_{ce}^2 v_{n\pm}^2/c^2 - n^2\omega_{ce}^2\left(1 - v_{\perp 0}^2/c^2\right) = 0. \tag{8}
$$

From perturbative theory, the real frequency is much higher than the growth rate ($|\omega_r| \gg |\gamma|$); thus $v_{n\pm}$ can be written as a function of ω_r as

$$
\frac{v_{n\pm}}{c} = \frac{\omega_r k_\parallel c \pm n\omega_{ce}\sqrt{\left(k_\parallel^2 c^2 + n^2\omega_{ce}^2\right)\left(1 - v_{\perp 0}^2/c^2\right) - \omega_r^2}}{k_\parallel^2 c^2 + n^2\omega_{ce}^2}. \tag{9}
$$

Here, $v_{n\pm}$ can have a real solution only for $\left(k_\parallel^2 c^2 + n^2\omega_{ce}^2\right)\left(1 - v_{\perp 0}^2/c^2\right) \geq \omega_r^2$; thus, we define a cutoff frequency ($\omega_{cut,n}$) for each harmonic number n as

$$
\omega_{cut,n}^2 \equiv \left(k_\parallel^2 c^2 + n^2\omega_{ce}^2\right)\left(1 - v_{\perp 0}^2/c^2\right). \tag{10}
$$

Since the O-mode real frequency is approximately given by the cold plasma dispersion relation, $\omega_{cut,n}^2 \approx \omega_{pe}^2 + k^2c^2$, where k is the wavenumber, the cutoff wave number perpendicular to $\mathbf{B}_0$ satisfying $\omega = \omega_{cut,n}$ is

$$
k_{cut,n} = \frac{\sqrt{\omega_{cut,n}^2 - \omega_{pe}^2}}{c}. \tag{11}
$$

Therefore, the wave-particle resonance occurs only when $\omega_r^2 < \omega_{cut,n}^2$ and $k_\perp < k_{cut,n}$, where $k_\perp$ is the real wavenumber perpendicular to $\mathbf{B}_0$. In addition, in dense plasma $\left(\omega_{pe}^2 \gg \omega_{ce}^2\right)$, such as near the plasmapause, when waves propagate strongly obliquely to $\mathbf{B}_0$ (i.e., $k_\parallel^2 \ll k_\perp^2$), a higher harmonic cyclotron number (n) is required for the appearance of particle resonance.

3. Resonant O-Mode Instabilities at the Plasmapause

We normalize the wave frequencies, velocities, and wavenumbers to ω_{ce}, the speed of light c, and $k_0 \equiv \omega_{ce}/c$, respectively. Then the normalized complex wave frequency ($\Omega \equiv \omega/\omega_{ce}$) can be described as a function of the normalized wavenumbers $K_{\perp(\parallel)} \equiv k_{\perp(\parallel)}/k_0$, total and hot electron plasma frequencies $\Omega_{pe(ph)} \equiv \omega_{pe(ph)}/\omega_{ce}$, normalized electron ring speed $V_{\perp 0} \equiv v_{\perp 0}/c$, parallel thermal speed $V_{e\parallel} \equiv v_{e\parallel}/c$, and parallel drift speed $U \equiv u/c$, respectively:

$$
\Omega = \Omega\left(K_\parallel, K_\perp, \Omega_{pe}, \Omega_h, V_{\perp 0}, V_{e\parallel}, U\right). \tag{12}
$$

We perform a numerical study to evaluate the influence of Ω_{pe}, $N_h \equiv n_h/n_e$, $V_{\perp 0}$, $V_{e\parallel}$, and U on wave growth rates. We use an empirical plasmasphere model (Gallagher et al., 1988, 2000) near the plasmapause and select physical parameters near $L = 2.5$ at the magnetic equator, which has been used in the previous NTC observations (Boardsen et al., 2023), of $\Omega_{pe} = 2-4$ and $N_h = 0.05-0.2$ for $K_p = 6$. Mildly energized electrons with $V_{\perp 0} = 0.1-0.4$ (equivalent to 10–40 keV electron energy), $V_{e\parallel} = 0.05-0.2$, and $U = 0-0.2$, are also considered.

We first demonstrate that the O-mode can be unstable because of the relativistic wave-particle resonance effect. Figures 1a and 1b show the normalized real frequency $\Omega_r \equiv \omega_r/\omega_{ce}$ and the corresponding wave growth rate $\Gamma \equiv \gamma/\omega_{ce}$ as a function of $K_\perp$ for a fixed $K_\parallel = 0.4$. Other parameters are $\Omega_{pe} = 3.5$, $N_h = 0.2$, $V_{\perp 0} = 0.4$, $V_{e\parallel} = 0.2$ and $U = 0$, respectively. The horizontal and vertical gray lines in the figure are $\Omega_{cut,n}$ and $K_{cut,n}$ from Equations 10 and 11 for various harmonic numbers of cyclotrons $4 \le n \le 9$, respectively.

Figure 1a shows that Ω_r increases with increasing $K_\perp$, and is almost identical to the frequency of the O-mode in the cold plasma approximation. In this figure, the thick red lines represent frequencies that are unstable. In Figure 1b, unstable O-modes have a weak growth rate in the narrow Ω_r and $K_\perp$ bands when both the conditions $\Omega_r^2 \le \Omega_{cut,n}^2$ and $K_\perp^2 \le K_{cut,n}^2$ for the same n cyclotron harmonic are satisfied. As anticipated in Section 2, higher harmonic cyclotron numbers are required for particle resonance in this dense plasma, and a strong Γ is seen for $n = 5$, 6, and 7, respectively. The corresponding harmonics in Ω_r are close to $n\omega_{ce}$. Maximum growth ($\Gamma_{\max}$) is observed for $n = 5$ at $\Omega \sim \Omega_{cut,n} \sim 4.59$ and $K \sim K_{cut,n} \sim 2.97$, close to, but not exactly, the same as the cutoff conditions. Here, the generated wave frequency is much higher than the frequency $\Omega_{LMC} \sim \Omega_{pe} = 3.5$ from the LMC theory.

Using Equation 8 we can calculate the resonant velocity $V_{n\pm}$ for each harmonic number n, as shown in Figure 1c. Black and magenta represent the $\pm$ signs, respectively. As $V_{n\pm}$ is a function of $(\Omega_{cut,r} - \Omega_r)$, it increases when Ω_r (and the corresponding $K_\perp$) decreases. When $\Gamma_{\max}$ occurs at $\Omega_r \sim \Omega_{cut,r}$, the resonant velocity can be approximated as

$$V_{n\pm} \sim \Omega_r K_\parallel / \left(K_\parallel^2 + n^2\right). \tag{13}$$

$\Gamma_{\max}$ is achieved for $n = 5$ and $V_{n\pm} = 0.073$ under the given conditions.

The angle of wave propagation $\left(\theta = \tan^{-1}\left(K_\perp/K_\parallel\right)\right)$ with respect to $\mathbf{B}_0$ increases as $K_\perp$ increases, as shown in Figure 1d. The values of θ with the highest growth rate are approximately 82.4° and 84.5° for $n = 5$ and 6, respectively, which is higher than the beaming angle of the LMC theory, $\theta_B = \tan^{-1}\sqrt{\Omega_{pe}} \approx 61°$. Thus, the O mode radiation directly generated via an energetic electron can propagate very close to perpendicular to $\mathbf{B}_0$.

We now investigate the influence of $K_\parallel$ on the resonance and growth rate. Figures 1e–1h show Ω_r and Γ as a function of $K_\parallel$ for fixed $K_\perp = 2.9$ and $n = 5$. The other parameters (Ω_{pe}, N_h, $V_{\perp 0}$, $V_{e\parallel}$, and U) remain the same as in Figures 1a–1d. Ω_r is nearly constant, slightly increasing from 4.548 to 4.549. Γ is positive only in the range of $0 < K_\parallel < 1$ and reaches its maximum value of $\Gamma \simeq 8 \times 10^{-6}$ at $\Omega_r \simeq 4.548$ and $K_\parallel \simeq 0.38$. Resonant parallel velocities $V_{n\pm}$ and wave propagation angle θ increase with $K_\parallel$, and when $\Gamma \to \Gamma_{\max}$, $V_{n\pm} \simeq 0.2$ and -0.0627, and $\theta \sim 83°$.

3.1. Plasma Density and Magnetic Field Effects

We investigate the influence of plasma density and magnetic field strength on the frequency of the O-mode and the growth rate. Figure 2a displays Ω_r in relation to $K_\perp$ for $\Omega_{pe} = 2$, 3, and 4, respectively, with the other fixed parameters ($K_\parallel$, N_h, $V_{\perp 0}$, $V_{e\parallel}$, and U) being the same as in Figures 1a–1d. Ω_r is almost the same as the frequency solutions obtained from the cold plasma wave dispersion, and it increases as Ω_{pe} increases.

We then plot Γ as a function of Ω_r in Figures 2b–2d for $\Omega_{pe} = 2$, 3, and 4, respectively. Since Ω_r is proportional to $K_\perp$ as shown in Figure 2a, the x axis in Figure 2b is also about $K_\perp$. In this figure, we first find that positive Γ occurs at higher Ω_r and n when Ω_{pe} increases. For example, $\Gamma > 0$ for $3 < n < 5$ and $\Omega_{pe} = 2$ and for $5 < n < 8$ and

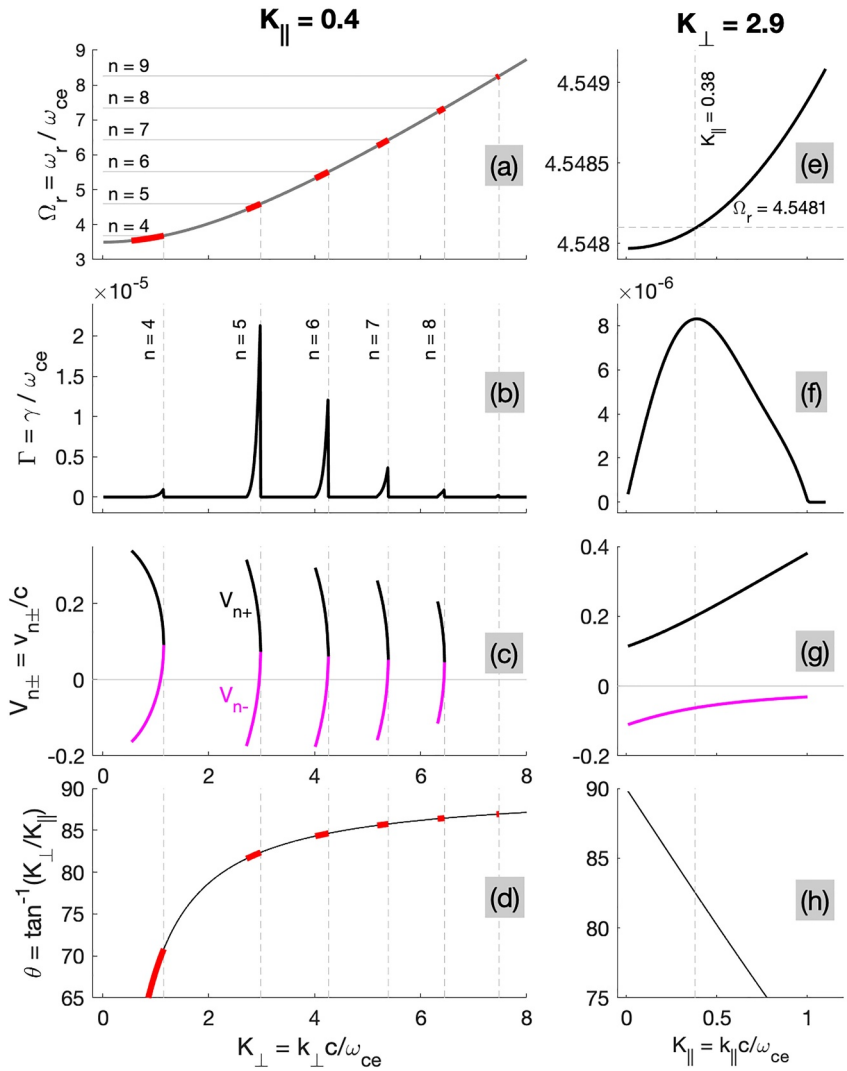

Figure 1. The calculated normalized real frequency $\Omega_r \equiv \omega_r/\omega_{ce}$, growth rate $\Gamma \equiv \gamma/\omega_{ce}$, normalized resonant wave velocity $V_{n\pm}$ and wave normal angle $\theta = \tan^{-1}(K_\perp/K_\parallel)$ as a function of (a–d) $K_\perp = k_\perp/k_0$ with $K_\parallel \equiv k_\parallel/c = 0.4$ and (e–h) $K_\parallel = k_\perp/k_0$ for $K_\perp = 2.9$. The physical parameters used are $\Omega_{pe} = 3.5$, $N_h \equiv n_h/n_e = 0.2$, $V_{\perp 0} \equiv v_{\perp 0}/c = 0.4$, $V_e \equiv v_e/c = 0.2$, and $U \equiv u/c = 0$, respectively. In the left column, the horizontal gray lines in (a) and the vertical gray lines in (a)–(d) represent the cutoff frequency $\Omega_{cut,n}$ and the wavenumber $K_{cut,n} \equiv k_{cut,n}c/\omega_{ce}$ for different cyclotron harmonic numbers n. The thick red lines in (a) and (d) indicate the regions where the waves are unstable, and the black and magenta lines in (c) and (e) are V_{n+} and V_{n-}, respectively. The vertical lines in the right column show the point at which the growth rate is maximized.

$\Omega_{pe} = 4$. The maximum growth rate Γ_{max} decreases as Ω_{pe} increases and shifts to higher Ω_r, $K_\perp$, and n; thus, Γ_{max} are 0.001, 9.5×10^{-5}, and 3.9×10^{-6} for $(\Omega_{pe}, \Omega_r, K_r, n) \sim (2, 2.77, 1.92, 3)$, $(3, 3.68, 2.13, 4)$, and $(4, 5.51, 3.7, 6)$, respectively. Near $\Gamma \sim \Gamma_{max}$, θ is ~78°, 79°, and 83°, which is larger than the LMC beaming angles $\theta_B = 55°$, 60°, and 63°, respectively, for $\Omega_{pe} = 2$, 3, and 4. $V_{n\pm}$ near Γ_{max} from Equation 13 is about 0.12, 0.09, and 0.06, which decreases as n increases.

The maximum growth rate Γ_{max} diminishes with increasing Ω_{pe} mainly because the resonant cyclotron harmonic number n increases, which can be seen from the asymptotic behavior of $J_n(x) \sim (x/2)^n/n!$ for $0 < x \ll \sqrt{n+1}$. For similar $k_\perp v_{\perp 0}/\omega_{ce}$ values, $J_n^2(k_\perp v_{\perp 0}/\omega_{ce})$ decreases with increasing n.

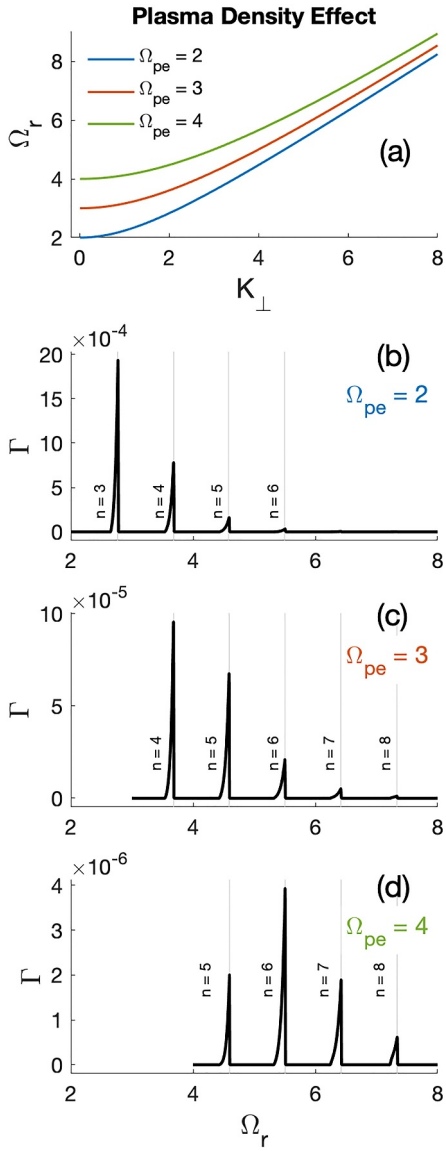

Figure 2. Plasma density effects on wave growth: (a) Ω_r versus $K_\perp$ and (b)–(d) Γ versus Ω_r when $K_\parallel = 0.4$ for $\Omega_{pe} = 2$, 3, and 4, respectively. The other fixed parameters are the same as in Figures 1a–1d, $N_h = 0.2$, $V_{\perp 0} = 0.4$, $V_{e\parallel} = 0.2$, $U = 0$, respectively. The vertical gray lines are $\Omega_{cut,n}$ for different cyclotron harmonic numbers n.

3.2. Suprathermal Electron Density Effects

We investigate how the suprathermal electron density affects the O-mode generation. We take three cases with N_h values of 0.05, 0.1, and 0.2, and assume that the total electron density (n_e) is the same in each case. Therefore, the Ω_r shown in Figure 3a is not influenced by the suprathermal density ratio and follows the wave dispersion relation in the cold plasma approximation.

At almost identical locations of $(\Omega_r, K_\perp)$, the waves become unstable in each case of varying N_h, as shown in Figure 3b. For a fixed $K_\parallel$ and $V_{\perp 0}$, $\Omega_{cut,r}$ is only a function of n; thus, $\Omega_{cut,n}$ is also independent of N_h. However, Γ is proportional to the suprathermal electron density, so Γ for $N_h = 0.1$ (and 0.2) is twice (and four times) higher than the one for $N_h = 0.05$, as seen in Figure 3b. Since $\Gamma \ll \Omega_r$, the perturbative approach of previous studies (Farrell, 2001; Freund & Wu, 1976) should give reasonably accurate results. The results in Figure 3 support the perturbative approach and the numerical results suggest that the growth rates can be scaled to other N_h values as long as $N_h \ll 1$.

3.3. Suprathermal Electron Velocity Distribution Effects

We explore the influence of suprathermal electron velocities on the real frequency Ω_r, growth rate Γ, and resonant velocity $V_{n\pm}$, as shown in Figure 4. The first, second, and third columns of the figure show the effects of the suprathermal ring speed ($V_{\perp 0}$), parallel thermal speed ($V_{e\parallel}$), and the drift speed (U), respectively.

Figure 4 plots (a) Ω_r versus $K_\perp$, (b)–(d) Γ versus $K_\perp$, and (e) $V_{n\pm}$ versus $K_\perp$, respectively, for $V_{\perp 0} = 0.1$, 0.2, and 0.4 (equivalent to 10, 20, and 40 keV electron energy). The figure shows that the real frequency is not significantly affected by $V_{\perp 0}$, but Γ changes drastically with $V_{\perp 0}$: $\Gamma_{\max}$ increases by a factor of 3×10^3 when $V_{\perp 0}$ increases from 0.1 to 0.4. In Figures 4b–4d, the vertical lines indicate $\Omega_{cut,n}$: $\Omega_{cut,n}$ is inversely proportional to $V_{\perp 0}$ for a fixed $K_\parallel$ and n as shown in Equation 10, thus the calculated $\Omega_{cut,n}$ decreases as $V_{\perp 0}$ increases. $\Gamma_{\max}$ shifts to higher n, occurring at $n = 4$ for $V_{\perp 0} = 0.1$, $n = 4$ for $V_{\perp 0} = 0.2$, and $n = 5$ for $V_{\perp 0} = 0.4$, respectively. Since $\Omega_{cut,n}$ decreases but Γ occurs at higher n numbers as $V_{\perp 0}$ increases, $\Gamma_{\max}$ does not vary monotonically with Ω_r and n, appearing at $\Omega_{cut,r} = 3.99$, 3.93, and 4.59, for $V_{\perp 0} = 0.1$, 0.2, and 0.4, respectively. In these cases, the resonant parallel speeds can be calculated in Figure 4e for $\Gamma_{\max}$, showing that they have similar values. Therefore, these results suggest that the main source of free energy is due to the suprathermal electron ring speed $V_{\perp 0}$ rather than the parallel resonance, and the increase of the maximum growth rate is mainly caused by the increase of $J_n^2(k_\perp v_{\perp 0}/\omega_{ce})$.

We now investigate the effect of the suprathermal electron parallel thermal speed ($V_{e\parallel}$). Figures 4e–4h show the variation of Ω_r with $K_\perp$ and of Γ with Ω_r for $V_{e\parallel} = 0.05$, 0.1, and 0.2. As in Figure 4a, Ω_r is independent of $V_{e\parallel}$ and is similar for these three cases. However, the maximum growth rates for these three cases are slightly different with $\Gamma_{\max} \simeq 6.5 \times 10^{-6}$, 2.7×10^{-5}, 2×10^{-5} for $V_{e\parallel} = 0.05$, 0.1, and 0.2 in Figures 4b–4d. $\Omega_{cut,n}$ is independent of $V_{e\parallel}$, so $\Omega_{cut,n}$ is also the same for each case, and the maximum $\Gamma_{\max}$ occurs at almost the same location in $(\Omega_r, K_\perp)$. Additionally, $V_{n\pm} = V_{n\pm}(\Omega_r, K_\parallel, n, \Omega_{cut,n})$ from Equation 9, so $V_{n\pm}$ is also almost the same for the given $K_\parallel$ and n at $\Omega \sim \Omega_{cut,n}$. Due to the plasma dispersion function $Z(\zeta_{n\pm}) = i\sqrt{\pi}\exp(-\zeta_{n\pm}^2) - 2\zeta_{n\pm}$ for $\zeta_{n\pm} \ll 1$, $\mathrm{Im}(Z(\zeta_{n\pm}))$ is inversely proportional to $\zeta_{n\pm}$. For $\Omega_r \sim \Omega_{cut,n}$, $\zeta_{n\pm} \sim \Omega_{cut,r}K_\parallel/\left(V_{e\parallel}\left(K_\parallel^2 + n^2\right)\right)$ from Equation 13, thus $\zeta_{n\pm}$ is also inversely proportional to $V_{e\parallel}$ for a constant $\Omega_{cut,n}$, $K_\parallel$ and n. Therefore, the difference in growth

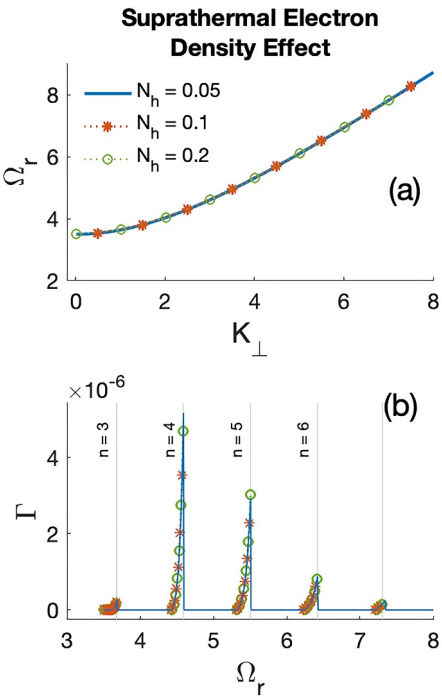

Figure 3. Suprathermal electron density effects on wave growth. (a) Ω_r and (b) Γ for $N_h = 0.05$ (blue), 0.1 (red), and 0.2 (green), respectively. Other parameters are the same as in Figure 1. The growth rates in (b) for each curve are scaled by factors of 1, 2, and 4, for $N_h = 0.05$, 0.1, and 0.2, respectively.

rate is mainly due to the change in the thermal spread in the suprathermal electron parallel velocity distribution, with larger $V_{e\|}$ leading to increased growth.

Finally, the effect of suprathermal electron parallel drift speed (U) is considered. In this case, Ω_r is almost independent of U, as shown in Figure 4j, and almost the same as in Figures 4a and 4f. As U increases, the maximum growth rate decreases slightly, with $\Gamma_{\max}$ approximately 2×10^{-5}, 1.25×10^{-5}, and 0.5×10^{-5} for $U = 0$, 0.1, and 0.2, respectively. When U becomes faster, Γ can be significant in a wider range of Ω_r, and the value of Ω_r with maximum Γ shifts to lower frequency: $\Gamma_{\max}$ occurs at $\Omega \sim \Omega_{cut,r} = 4.59$ for $U = 0$ and 0.1 but occurs at $\Omega \sim 4.54$ for $U = 0.2$. For $\Gamma \sim \Gamma_{\max}$, $V_{n\pm}$ is ~ 0.073 for $U = 0$ and $U_e = 0.1$ and increases to 0.21 for $U = 0.2$. Consequently, the difference in the growth rate is mainly due to the change in the parallel drift speed.

4. Summary and Discussion

From our studies of the O-mode instability for different core plasma and suprathermal electron parameters, we found that the O-mode can be destabilized via the semi-relativistic wave-particle resonance by suprathermal electron velocity space free energy sources in low β plasma conditions. In this paper, we perform numerical calculations of the O-mode instability for a ring beam velocity distribution of suprathermal electrons. For the suprathermal electron ring velocity distribution at $v_{\perp 0}$, to satisfy the semi-relativistic wave-particle resonance condition for a given cyclotron harmonic n, the wave frequency and the perpendicular wave vector must satisfy $\omega_r^2 \le \omega_{cut,n}^2$ and $k_\perp^2 \le k_{cut,n}^2$, where $\omega_{cut,n}^2 = \left(k_\|^2 c^2 + n^2 \omega_{ce}^2\right)\left(1 - v_{\perp 0}^2/c^2\right)$ and $k_{cut,n}^2 c^2 = \omega_{cut,n}^2 - \omega_{pe}^2$.

We found that resonant O-modes are unstable over multiple narrow frequency and wavevector ranges. Typically, the growth rate rapidly increases as cyclotron harmonic number n increases and gradually decreases after it reaches the maximum value. For a fixed $k_\|$, the wave frequency increases with $k_\perp$. Because $k_\perp > k_\|$, this implies that the O-mode propagation angle is close to 90° with respect to the ambient magnetic field. The most important parameters that determine the magnitude of the growth rate are the density of the core plasma frequency to the electron cyclotron frequency, ω_{pe}/ω_{ce}, the suprathermal electron ring speed $v_{\perp 0}/c$, and the density n_h/n_e. The growth rate is weak for these resonant O-mode instabilities with γ/ω_r in the range of $10^{-9} - 10^{-5}$ for $n_h/n_e \simeq 0.05 - 0.2$, $\omega_{pe}/\omega_{ce} \simeq 2 - 4$, $v_{\perp 0}/c \simeq 0.1 - 0.4$, $v_{e\|}/c \simeq 0.05 - 0.2$, and $u/c \simeq 0 - 0.2$.

This study focuses on analyzing the O-mode instability without considering the competing instability of the electrostatic mode. However, in cases where the growth rate of the electrostatic modes is significantly higher than that of O-mode waves, the electrostatic waves quickly change the velocity distribution within the wave source at a rate that exceeds the growth rate of the O-mode waves. Consequently, this effect should be the subject of future investigation.

Plasmapause parameters typically have ω_{pe}/ω_{ce} in the range of $1 - 5$, $n_h/n_e \simeq 0.001 - 0.1$, and $v_{\perp 0}/c \approx 0.2$ for electron energy at 20 keV. Therefore, the numerical results in Section 3 are relevant to the plasmapause situation. The numerical solutions indicate that multiple harmonic structures of the NTC (Décréau et al., 2015; Grimald & Santolík, 2010; Morgan & Gurnett, 1991) with harmonic spacings $\simeq \omega_{ce}$ can be supported by the resonant O-mode excited in the plasmapause region. Moreover, the O modes exhibit a beaming angle close to 90° with respect to the magnetic field in the plasmapause region, which is much higher than that predicted by the LMC theory. The electron gyrofrequency at the plasmapause near $L = 2.5$ can be approximated by $f_{ce} = \omega_{ce}/2\pi \sim 56$ kHz using the dipole model. In this case, the corresponding wave frequency ranges from 112 to 336 kHz for a normalized frequency Ω_r between 2 and 6. The results of this study show good agreement with previous observational findings that the detected wave beaming angle is much higher than the theoretical values of the LMC theory

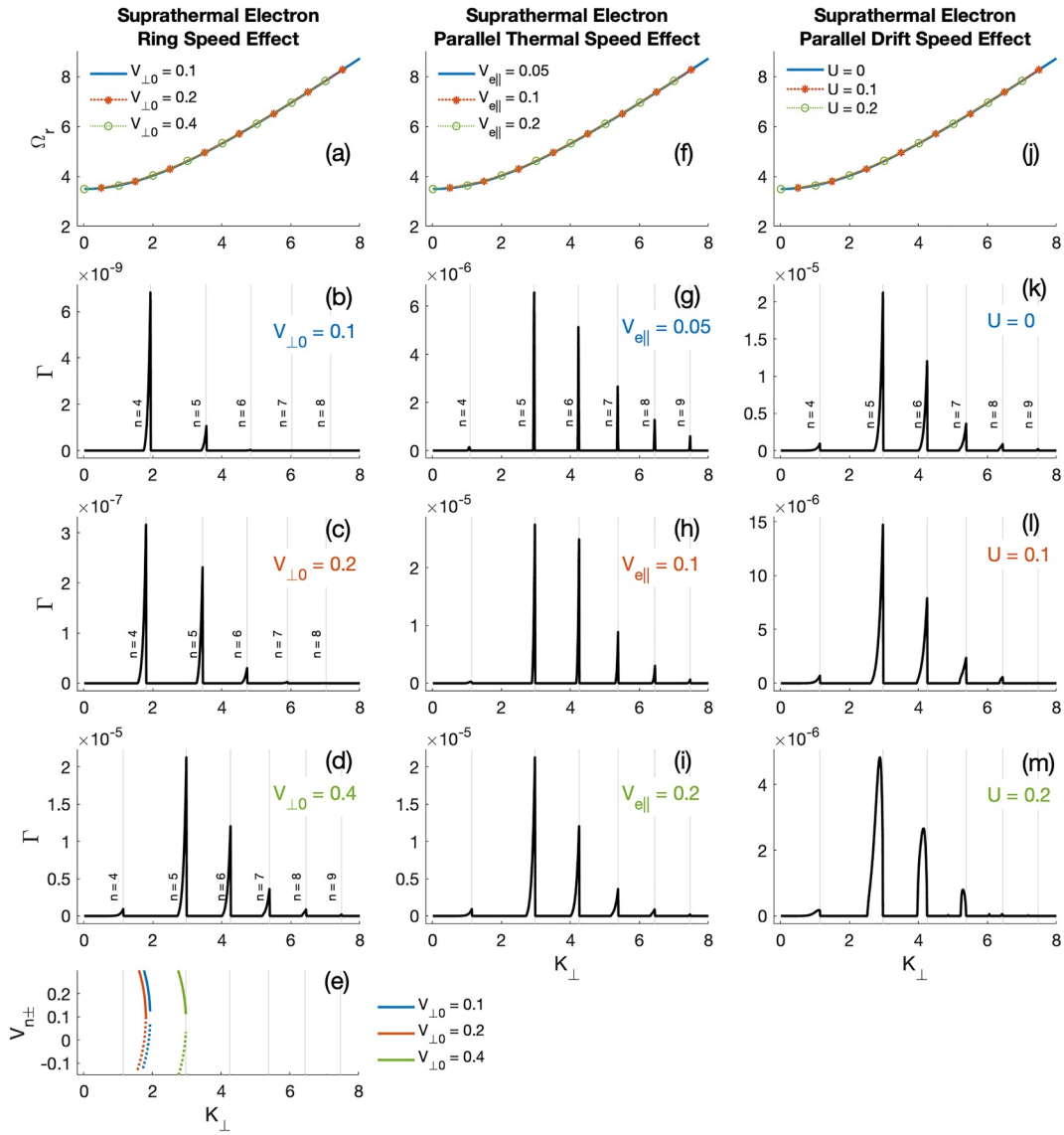

Figure 4. (a)–(e) Suprathermal electron ring speed effect for (a)–(d) $V_\perp = 0.1$, 0.2, and 0.4, (f)–(i) suprathermal electron parallel thermal speed effect for $V_{e\|} = 0.05$, 0.1, and 0.2, and (j)–(k) suprathermal electron parallel drift speed effect for $U = 0$, 0.1, and 0.2, respectively. The first row is Ω_r versus $K_\perp$, the second to fourth rows are Γ versus $K_\perp$, and the fifth row is $V_{n\pm}$ versus $K_\perp$, respectively. The other fixed parameters are the same as Figures 1a–1d.

(Boardsen et al., 2008, 2023; Hashimoto et al., 2005). Specifically, the findings strongly support the recent statistical study that the NTC radiation beam angle for the higher frequency range (100–400 kHz) is close to 90° (Boardsen et al., 2023). The results are also similar to the previous direct generation mechanism (Farrell, 2001), which used bi-Maxwellian distributions of electrons to produce instability.

The lower frequency NTC with frequencies between 51 and 100 kHz, Boardsen et al. (2023) obviously supports the LMC theory; however, these NTCs are also detected near the magnetic equator with a wave beaming angle of approximately 90°. Assuming the same suprathermal electron conditions, the maximum growth rate is expected to occur near $\Omega_r \sim 4.5$. This suggests that lower-frequency NTC radiations with frequencies between 50 and 100 kHz can be generated at an outer L-shell, and it can be estimated that it occurs near the magnetic equator at $3 < L < 4$. However, for more precise results, further calculations should be performed.

Data Availability Statement

The data on which this article is based are available in Cheng et al. (2023). The Zip file includes eight directories (Figxx) in the directory. Each directory number xx represents the figure numbers and includes Matlab data or binary text files and Matlab source files that can reproduce the figures.

Acknowledgments
The authors thank the reviewers for the helpful discussion. This paper is based on work supported by the US Department of Energy, Office of Science, Office of Fusion Energy Sciences under contract DE-AC02-09CH11466. The authors acknowledge support from the National Science Foundation (NSF) Grant AGS 2131013 and NASA Grants 80HQTR18T0066, 80HQTR19T0076, and 80NSSC22K0515. This work was also partially funded by NASA through the GPHI Cooperative Agreement NNG11PL02A and PHASER 80NSSC21M0180, and by the Australian Research Council Grant DP18103509.

References

Boardsen, S. A., Green, J. L., & Reinisch, B. W. (2008). Comparison of kilometric continuum latitudinal radiation patterns with linear mode conversion theory. *Journal of Geophysical Research*, *113*(A1), A01219. https://doi.org/10.1029/2007JA012319

Boardsen, S. A., Kim, E.-H., Green, J. L., Cheng, C. Z., Cairns, I. H., & Johnson, J. R. (2023). Statistical study of the nonthermal continuum radiation beaming angle measured by the high frequency receiver on Van Allen Probes-A. *Journal of Geophysical Research: Space Physics*, *128*(9), e2023JA031426. https://doi.org/10.1029/2023JA031426

Budden, K. G. (1980). The theory of radio windows in the ionosphere and magnetosphere. *Journal of Atmospheric and Terrestrial Physics*, *42*(3), 287–298. https://doi.org/10.1016/0021-9169(80)90036-7

Budden, K. G., & Jones, D. (1987). Conversion of electrostatic upper hybrid emissions to electromagnetic O and X mode waves in the Earth's magnetosphere. *Annales Geophysicae*, *5*, 21–28.

Cheng, C. Z. (1975). Ordinary electromagnetic mode instability. *Journal of Plasma Physics*, *13*(2), 335–346. https://doi.org/10.1017/s002237780002609x

Cheng, C. Z., Kim, E.-H., Boardsen, S. A., Cairns, I. H., & Johnson, J. R. (2023). *O-Mode instability for non-thermal continuum radiation generated near the plasmapause*. Princeton Plasma Physics Laboratory, Princeton University. https://doi.org/10.34770/jvhk-3861

Décréau, P. M. E., Aoutou, S., Denazelle, A., Galkina, I., Rauch, J.-L., Vallières, X., et al. (2015). Wide-banded NTC radiation: Local to remote observations by the four Cluster satellites. *Annales Geophysicae*, *33*(10), 1285–1300. https://doi.org/10.5194/angeo-33-1285-2015

Décréau, P. M. E., Ducoin, C., Rouzic, G. L., Randriamboarison, O., Rauch, J.-L., Trotignon, J.-G., et al. (2004). Observation of continuum radiations from the Cluster fleet: First results from direction finding. *Annales Geophysicae*, *22*, 2607. https://doi.org/10.5194/angeo-22-2607-2004

Farrell, W. M. (2001). Direct generation of O-mode emission in a dense, warm plasma: Applications to interplanetary type II emissions and others in its class. *Journal of Geophysical Research*, *106*(A8), 15701–15709. https://doi.org/10.1029/2000ja000156

Freund, H. P., & Wu, C. S. (1976). Excitation of the ordinary electromagnetic mode in low-β plasmas. *The Physics of Fluids*, *19*(2), 299–304. https://doi.org/10.1063/1.861440

Fung, S. F., & Papadopoulos, K. (1987). The emission of narrow-band Jovian kilometric radiation. *Journal of Geophysical Research*, *92*(A8), 8579–8593. https://doi.org/10.1029/JA092iA08p08579

Gaffey, J. D., Thompson, W. B., & Liu, C. S. (1972). Ordinary-mode electromagnetic instability for counter-streaming plasmas with anisotropic temperatures. *Journal of Plasma Physics*, *7*(2), 189–206. https://doi.org/10.1017/S002237780000653X

Gaffey, J. D., Thompson, W. B., & Liu, C. S. (1973). Ordinary-mode electromagnetic instability for counter-streaming ions with anisotropic temperatures. *Journal of Plasma Physics*, *9*(1), 17–21. https://doi.org/10.1017/S0022377800007297

Gallagher, D. L., Craven, P. D., & Comfort, R. H. (1988). An empirical model of the Earth's plasmasphere. *Advances in Space Research*, *8*(8), 15–24. https://doi.org/10.1016/0273-1177(88)90258-X

Gallagher, D. L., Craven, P. D., & Comfort, R. H. (2000). Global core plasma model. *Journal of Geophysical Research*, *105*(A8), 18819–18833. https://doi.org/10.1029/1999ja000241

Green, J. L., & Boardsen, S. (1999). Confinement of nonthermal continuum radiation to low latitudes. *Journal of Geophysical Research*, *104*, 10307. https://doi.org/10.1029/1998JA900130

Green, J. L., Boardsen, S. A., Fung, S. F., Matsumoto, H., Hashimoto, K., Anderson, R. R., et al. (2004). Association of kilometric continuum radiation with plasmaspheric structures. *Journal of Geophysical Research*, *109*(A3), A03203. https://doi.org/10.1029/2003JA010093

Green, J. L., Sandel, B., Fung, S., Gallagher, D., & Reinisch, B. (2002). On the origin of kilometric continuum. *Journal of Geophysical Research*, *107*(A7), SMP 12-1–SMP 12-10. https://doi.org/10.1029/2001JA000193

Grimald, S., Décréau, P. M. E., Canu, P., Suraud, X., Vallières, X., Darrouzet, F., & Harvey, C. C. (2007). A quantitative test of Jones NTC beaming theory using CLUSTER constellation. *Annales Geophysicae*, *25*(3), 823–831. https://doi.org/10.5194/angeo-25-823-2007

Grimald, S., & Santolík, O. (2010). Possible wave modes of wideband nonthermal continuum radiation in its source region. *Journal of Geophysical Research*, *115*(A6), A06209. https://doi.org/10.1029/2009JA014997

Gurnett, D. A. (1975). The Earth as a radio source: The nonthermal continuum. *Journal of Geophysical Research*, *80*(19), 2751–2763. https://doi.org/10.1029/JA080i019p02751

Gurnett, D. A., Calvert, W., Huff, R. L., Jones, D., & Sugiu, M. (1988). The polarization of escaping terrestrial continuum radiation. *Journal of Geophysical Research*, *93*(A11), 12817–12825. https://doi.org/10.1029/ja093ia11p12817

Hashimoto, K., Anderson, R., Green, J., & Matsumoto, H. (2005). Source and Propagation Characteristics of kilometric continuum observed with multiple satellite. *Journal of Geophysical Research*, *110*(A9), A09229. https://doi.org/10.1029/2004JA010729

Hashimoto, K., Calvert, W., & Matsumoto, H. (1999). Kilometric continuum detected by Geotail. *Journal of Geophysical Research*, *104*(A12), 28645–28656. https://doi.org/10.1029/1999ja900365

Horký, M., & Omura, Y. (2019). Novel nonlinear mechanism of the generation of non-thermal continuum radiation. *Physics of Plasmas*, *26*(2), 022904. https://doi.org/10.1063/1.5077094

Horký, M., Omura, Y., & Santolík, O. (2018). Particle simulation of electromagnetic emissions from electrostatic instability driven by an electron ring beam on the density gradient. *Physics of Plasmas*, *25*(4), 042905. https://doi.org/10.1063/1.5025912

Jones, D. (1980). Latitudinal beaming of planetary radio emissions. *Nature*, *288*(5788), 225–229. https://doi.org/10.1038/288225a0

Jones, D., Calvert, W., Gurnett, D. A., & Huff, R. L. (1987). Observed beaming of terrestrial myriametric radiation. *Nature*, *328*(23), 391–395. https://doi.org/10.1038/328391a0

Kalaee, M. J., & Katoh, Y. (2016a). The role of deviation of magnetic field direction on the beaming angle: Extending of beaming angle theory. *Journal of Atmospheric and Solar-Terrestrial Physics*, *142*, 35–42. https://doi.org/10.1016/j.jastp.2016.02.021

Kalaee, M. J., & Katoh, Y. (2016b). Study of a condition for the mode conversion from purely perpendicular electrostatic waves to electromagnetic waves. *Physics of Plasmas*, *23*(7), 072119. https://doi.org/10.1063/1.4958945

Kalaee, M. J., & Katoh, Y. (2020). Plasma frequency demand for mode conversion processes from slow Z-mode to LO-mode waves in an inhomogeneous plasma. *Earth, Planets and Space*, *72*(1), 95. https://doi.org/10.1186/s40623-020-01226-x

Kalaee, M. J., Katoh, Y., & Ono, T. (2014). Effects of the angle between the density gradient and the external magnetic field on the linear mode conversion and resultant beaming angle of LO-mode radio emissions. *Earth, Moon, and Planets*, *114*(1), 1–15. https://doi.org/10.1007/s11038-014-9448-4

Kasaba, Y., Matsumoto, H., Hashimoto, K., Anderson, R. R., Bougeret, J.-L., Kaiser, M. L., et al. (1998). Remote sensing of the plasmapause during substorms: Geotail observation of nonthermal continuum enhancement. *Journal of Geophysical Research*, *103*(A9), 20389–20405. https://doi.org/10.1029/98ja00809

Kim, E.-H., Cairns, I. H., & Johnson, J. R. (2013). Linear mode conversion of Langmuir/z-mode waves to radiation in plasmas with various magnetic field strength. *Physics of Plasmas*, *20*(12), 122103. https://doi.org/10.1063/1.4837515

Kim, E.-H., Cairns, I. H., & Robinson, P. A. (2007). Extraordinary-mode radiation produced by linear-mode conversion of Langmuir waves. *Physical Review Letters*, *99*(1), 015003. https://doi.org/10.1103/PhysRevLett.99.015003

Kim, E.-H., Cairns, I. H., & Robinson, P. A. (2008). Mode conversion of Langmuir to electromagnetic waves at magnetic field-aligned density inhomogeneities: Simulations, theory, and applications to the solar wind and the corona. *Physics of Plasmas*, *15*(10), 102110. https://doi.org/10.1063/1.2994719

Kurth, W. S., Ashour-Abdalla, M., Frank, L. A., Kennel, C. F., Gurnett, D. A., Sentman, D. D., & Burek, B. G. (1979). A comparison of intense electrostatic waves near fUHR with linear instability theory. *Geophysical Research Letters*, *6*(6), 487–490. https://doi.org/10.1029/GL006i006p00487

Kurth, W. S., Frank, L. A., Ashour-Abdalla, M., Gurnett, D. A., & Burek, B. G. (1980). Observations of a free-energy source for intense electrostatic waves. *Geophysical Research Letters*, *7*(5), 293–296. https://doi.org/10.1029/GL007i005p00293

Kurth, W. S., & Gurnett, D. A. (1991). Plasma waves in planetary magnetospheres. *Journal of Geophysical Research*, *96*(S01), 18977–18991. https://doi.org/10.1029/91JA01819

Kurth, W. S., Gurnett, D. A., & Anderson, R. R. (1981). Escaping nonthermal continuum radiation. *Journal of Geophysical Research*, *86*(A7), 5519–5531. https://doi.org/10.1029/ja086ia07p05519

Kurth, W. S., Hospodarsky, G. B., Gurnett, D. A., Lamy, L., Dougherty, M. K., Nichols, J., et al. (2016). Saturn kilometric radiation intensities during the Saturn auroral campaign of 2013. *Icarus*, *263*, 2–9. https://doi.org/10.1016/j.icarus.2015.01.003

Louis, C. K., Zarka, P., Dabidin, K., Lampson, P.-A., Magalhães, F. P., Boudouma, A., et al. (2021). Latitudinal beaming of Jupiter's radio emissions from Juno/Waves flux density measurements. *Journal of Geophysical Research: Space Physics*, *126*(10), e2021JA029435. https://doi.org/10.1029/2021JA029435

Melrose, D. B. (1981). A theory for the nonthermal radio continuum in the terrestrial and Jovian magnetospheres. *Journal of Geophysical Research*, *86*(A1), 30–36. https://doi.org/10.1029/ja086ia01p00030

Morgan, D. D., & Gurnett, D. A. (1991). The source location and beaming of terrestrial continuum radiation. *Journal of Geophysical Research*, *96*(A6), 9595–9613. https://doi.org/10.1029/91ja00314

Oya, H. (1971). Conversion of electrostatic waves into electromagnetic waves: Numerical calculation of the dispersion relation for all wavelengths. *Radio Science*, *6*(12), 1131–1141. https://doi.org/10.1029/rs006i012p01131

Rönnmark, K. (1983). Emission of myriametric radiation by coalescence of upper hybrid waves with low frequency waves. *Annales Geophysicae*, *1*, 187.

Schleyer, F., Cairns, I. H., & Kim, E.-H. (2013). Linear mode conversion of Langmuir/z-mode waves to radiation: Scalings of conversion efficiencies and propagation angles with temperature and magnetic field orientation. *Physics of Plasmas*, *20*(3), 032101. https://doi.org/10.1063/1.4793726

Schleyer, F., Cairns, I. H., & Kim, E.-H. (2014). Linear mode conversion of Langmuir/z mode waves to radiation: Averaged energy conversion efficiencies, polarization, and applications to Earth's continuum radiation. *Journal of Geophysical Research: Space Physics*, *119*(5), 3392–3410. https://doi.org/10.1002/2013JA019364

Sentman, D. D., Frank, L. A., Gurnett, D. A., Kurth, W. S., & Kennel, C. F. (1979). Electron distribution functions associated with electrostatic emissions in the dayside magnetosphere. *Geophysical Research Letters*, *6*(10), 781–784. https://doi.org/10.1029/GL006i010p00781

Shi, B. R., Gaffey, J. D., Jr., & Wu, C. S. (1986). Amplification of electromagnetic waves by a ring–beam distribution of moderately relativistic electrons. *The Physics of Fluids*, *29*(12), 4212–4218. https://doi.org/10.1063/1.865712

Wu, C. S., & Lee, L. C. (1979). A theory of the terrestrial kilometric radiation. *The Astrophysical Journal*, *230*, 621. https://doi.org/10.1086/157120

Wu, S. Y., Ye, S. Y., Fischer, G., Jackman, C. M., Wang, J., Menietti, J. D., et al. (2022). Reflection and refraction of the L-O mode 5 kHz Saturn narrowband emission by the magnetosheath. *Geophysical Research Letters*, *49*(5), e2021GL096990. https://doi.org/10.1029/2021GL096990

Ye, S.-Y., Gurnett, D. A., Fischer, G., Cecconi, B., Menietti, J. D., Kurth, W. S., et al. (2009). Source locations of narrowband radio emissions detected at Saturn. *Journal of Geophysical Research*, *114*(A6), A06219. https://doi.org/10.1029/2008JA013855

Ye, S.-Y., Menietti, J. D., Fischer, G., Wang, Z., Cecconi, B., Gurnett, D. A., & Kurth, W. S. (2010). Z mode waves as the source of Saturn narrowband radio emissions. *Journal of Geophysical Research*, *115*(A8), A08228. https://doi.org/10.1029/2009JA015167